

Measurement of the Branching Fraction For the Semileptonic Decay $D^{0(+)} \rightarrow \pi^{-(0)} \mu^+ \nu_\mu$ and Test of Lepton Flavor Universality

M. Ablikim,¹ M. N. Achasov,^{9,d} S. Ahmed,¹⁴ M. Albrecht,⁴ A. Amoroso,^{53a,53c} F. F. An,¹ Q. An,^{50,40} J. Z. Bai,¹ Y. Bai,³⁹ O. Bakina,²⁴ R. Baldini Ferroli,^{20a} Y. Ban,³² D. W. Bennett,¹⁹ J. V. Bennett,⁵ N. Berger,²³ M. Bertani,^{20a} D. Bettoni,^{21a} J. M. Bian,⁴⁷ F. Bianchi,^{53a,53c} E. Boger,^{24,b} I. Boyko,²⁴ R. A. Briere,⁵ H. Cai,⁵⁵ X. Cai,^{1,40} O. Cakir,^{43a} A. Calcaterra,^{20a} G. F. Cao,^{1,44} S. A. Cetin,^{43b} J. Chai,^{53c} J. F. Chang,^{1,40} G. Chelkov,^{24,b,c} G. Chen,¹ H. S. Chen,^{1,44} J. C. Chen,¹ M. L. Chen,^{1,40} P. L. Chen,⁵¹ S. J. Chen,³⁰ X. R. Chen,²⁷ Y. B. Chen,^{1,40} X. K. Chu,³² G. Cibinetto,^{21a} H. L. Dai,^{1,40} J. P. Dai,^{35,h} A. Dbeyssi,¹⁴ D. Dedovich,²⁴ Z. Y. Deng,¹ A. Denig,²³ I. Denysenko,²⁴ M. Destefanis,^{53a,53c} F. De Mori,^{53a,53c} Y. Ding,²⁸ C. Dong,³¹ J. Dong,^{1,40} L. Y. Dong,^{1,44} M. Y. Dong,^{1,40,44} Z. L. Dou,³⁰ S. X. Du,⁵⁷ P. F. Duan,¹ J. Fang,^{1,40} S. S. Fang,^{1,44} Y. Fang,¹ R. Farinelli,^{21a,21b} L. Fava,^{53b,53c} S. Fegan,²³ F. Feldbauer,²³ G. Felici,^{20a} C. Q. Feng,^{50,40} E. Fioravanti,^{21a} M. Fritsch,^{23,14} C. D. Fu,¹ Q. Gao,¹ X. L. Gao,^{50,40} Y. Gao,⁴² Y. G. Gao,⁶ Z. Gao,^{50,40} I. Garzia,^{21a} K. Goetzen,¹⁰ L. Gong,³¹ W. X. Gong,^{1,40} W. Gradl,²³ M. Greco,^{53a,53c} M. H. Gu,^{1,40} Y. T. Gu,¹² A. Q. Guo,¹ R. P. Guo,^{1,44} Y. P. Guo,²³ Z. Haddadi,²⁶ S. Han,⁵⁵ X. Q. Hao,¹⁵ F. A. Harris,⁴⁵ K. L. He,^{1,44} X. Q. He,⁴⁹ F. H. Heinsius,⁴ T. Held,⁴ Y. K. Heng,^{1,40,44} T. Holtmann,⁴ Z. L. Hou,¹ H. M. Hu,^{1,44} T. Hu,^{1,40,44} Y. Hu,¹ G. S. Huang,^{50,40} J. S. Huang,¹⁵ X. T. Huang,³⁴ X. Z. Huang,³⁰ Z. L. Huang,²⁸ T. Hussain,⁵² W. Ikegami Andersson,⁵⁴ Q. Ji,¹ Q. P. Ji,¹⁵ X. B. Ji,^{1,44} X. L. Ji,^{1,40} X. S. Jiang,^{1,40,44} X. Y. Jiang,³¹ J. B. Jiao,³⁴ Z. Jiao,¹⁷ D. P. Jin,^{1,40,44} S. Jin,^{1,44} Y. Jin,⁴⁶ T. Johansson,⁵⁴ A. Julin,⁴⁷ N. Kalantar-Nayestanaki,²⁶ X. L. Kang,¹ X. S. Kang,³¹ M. Kavatsyuk,²⁶ B. C. Ke,⁵ T. Khan,^{50,40} A. Khoukaz,⁴⁸ P. Kiese,²³ R. Kliemt,¹⁰ L. Koch,²⁵ O. B. Kolcu,^{43b,f} B. Kopf,⁴ M. Kornicer,⁴⁵ M. Kuemmel,⁴ M. Kuessner,⁴ M. Kuhlmann,⁴ A. Kupsc,⁵⁴ W. Kühn,²⁵ J. S. Lange,²⁵ M. Lara,¹⁹ P. Larin,¹⁴ L. Lavezzi,^{53c} H. Leithoff,²³ C. Leng,^{53c} C. Li,⁵⁴ Cheng Li,^{50,40} D. M. Li,⁵⁷ F. Li,^{1,40} F. Y. Li,³² G. Li,¹ H. B. Li,^{1,44} H. J. Li,^{1,44} J. C. Li,¹ Jin Li,³³ K. J. Li,⁴¹ Kang Li,¹³ Ke Li,³⁴ Lei Li,³ P. L. Li,^{50,40} P. R. Li,^{44,7} Q. Y. Li,³⁴ W. D. Li,^{1,44} W. G. Li,¹ X. L. Li,³⁴ X. N. Li,^{1,40} X. Q. Li,³¹ Z. B. Li,⁴¹ H. Liang,^{50,40} Y. F. Liang,³⁷ Y. T. Liang,²⁵ G. R. Liao,¹¹ D. X. Lin,¹⁴ B. Liu,^{35,h} B. J. Liu,¹ C. X. Liu,¹ D. Liu,^{50,40} F. H. Liu,³⁶ Fang Liu,¹ Feng Liu,⁶ H. B. Liu,¹² H. M. Liu,^{1,44} Huanhuan Liu,¹ Huihui Liu,¹⁶ J. B. Liu,^{50,40} J. P. Liu,⁵⁵ J. Y. Liu,^{1,44} K. Liu,⁴² K. Y. Liu,²⁸ Ke Liu,⁶ L. D. Liu,³² P. L. Liu,^{1,40} Q. Liu,⁴⁴ S. B. Liu,^{50,40} X. Liu,²⁷ Y. B. Liu,³¹ Z. A. Liu,^{1,40,44} Zhiqing Liu,²³ Y. F. Long,³² X. C. Lou,^{1,40,44} H. J. Lu,¹⁷ J. G. Lu,^{1,40} Y. Lu,¹ Y. P. Lu,^{1,40} C. L. Luo,²⁹ M. X. Luo,⁵⁶ X. L. Luo,^{1,40} X. R. Lyu,⁴⁴ F. C. Ma,²⁸ H. L. Ma,¹ L. L. Ma,³⁴ M. M. Ma,^{1,44} Q. M. Ma,¹ T. Ma,¹ X. N. Ma,³¹ X. Y. Ma,^{1,40} Y. M. Ma,³⁴ F. E. Maas,¹⁴ M. Maggiora,^{53a,53c} Q. A. Malik,⁵² Y. J. Mao,³² Z. P. Mao,¹ S. Marcello,^{53a,53c} Z. X. Meng,⁴⁶ J. G. Messchendorp,²⁶ G. Mezzadri,^{21b} J. Min,^{1,40} T. J. Min,¹ R. E. Mitchell,¹⁹ X. H. Mo,^{1,40,44} Y. J. Mo,⁶ C. Morales Morales,¹⁴ N. Yu. Muchnoi,^{9,d} H. Muramatsu,⁴⁷ P. Musiol,⁴ A. Mustafa,⁴ Y. Nefedov,²⁴ F. Nerling,¹⁰ I. B. Nikolaev,^{9,d} Z. Ning,^{1,40} S. Nisar,⁸ S. L. Niu,^{1,40} X. Y. Niu,^{1,44} S. L. Olsen,^{33,j} Q. Ouyang,^{1,40,44} S. Pacetti,^{20b} Y. Pan,^{50,40} M. Papenbrock,⁵⁴ P. Patteri,^{20a} M. Pelizaeus,⁴ J. Pellegrino,^{53a,53c} H. P. Peng,^{50,40} K. Peters,^{10,g} J. Pettersson,⁵⁴ J. L. Ping,²⁹ R. G. Ping,^{1,44} A. Pitka,²³ R. Poling,⁴⁷ V. Prasad,^{50,40} H. R. Qi,² M. Qi,³⁰ S. Qian,^{1,40} C. F. Qiao,⁴⁴ N. Qin,⁵⁵ X. S. Qin,⁴ Z. H. Qin,^{1,40} J. F. Qiu,¹ K. H. Rashid,^{52,i} C. F. Redmer,²³ M. Richter,⁴ M. Ripka,²³ M. Rolo,^{53c} G. Rong,^{1,44} Ch. Rosner,¹⁴ A. Sarantsev,^{24,e} M. Savrié,^{21b} C. Schnier,⁴ K. Schoenning,⁵⁴ W. Shan,³² M. Shao,^{50,40} C. P. Shen,² P. X. Shen,³¹ X. Y. Shen,^{1,44} H. Y. Sheng,¹ J. J. Song,³⁴ W. M. Song,³⁴ X. Y. Song,¹ S. Sosio,^{53a,53c} C. Sowa,⁴ S. Spataro,^{53a,53c} G. X. Sun,¹ J. F. Sun,¹⁵ L. Sun,⁵⁵ S. S. Sun,^{1,44} X. H. Sun,¹ Y. J. Sun,^{50,40} Y. K. Sun,^{50,40} Y. Z. Sun,¹ Z. J. Sun,^{1,40} Z. T. Sun,¹⁹ C. J. Tang,³⁷ G. Y. Tang,¹ X. Tang,¹ I. Tapan,^{43c} M. Tiemens,²⁶ B. Tsednee,²² I. Uman,^{43d} G. S. Varner,⁴⁵ B. Wang,¹ B. L. Wang,⁴⁴ D. Wang,³² D. Y. Wang,³² Dan Wang,⁴⁴ K. Wang,^{1,40} L. L. Wang,¹ L. S. Wang,¹ M. Wang,³⁴ Meng Wang,^{1,44} P. Wang,¹ P. L. Wang,¹ W. P. Wang,^{50,40} X. F. Wang,⁴² Y. Wang,^{50,40,38} Y. D. Wang,¹⁴ Y. F. Wang,^{1,40,44} Y. Q. Wang,²³ Z. Wang,^{1,40} Z. G. Wang,^{1,40} Z. Y. Wang,¹ Zongyuan Wang,^{1,44} T. Weber,²³ D. H. Wei,¹¹ P. Weidenkaff,²³ S. P. Wen,¹ U. Wiedner,⁴ M. Wolke,⁵⁴ L. H. Wu,¹ L. J. Wu,^{1,44} Z. Wu,^{1,40} L. Xia,^{50,40} Y. Xia,¹⁸ D. Xiao,¹ H. Xiao,⁵¹ Y. J. Xiao,^{1,44} Z. J. Xiao,²⁹ Y. G. Xie,^{1,40} Y. H. Xie,⁶ X. A. Xiong,^{1,44} Q. L. Xiu,^{1,40} G. F. Xu,¹ J. J. Xu,^{1,44} L. Xu,¹ Q. J. Xu,¹³ Q. N. Xu,⁴⁴ X. P. Xu,³⁸ L. Yan,^{53a,53c} W. B. Yan,^{50,40} W. C. Yan,² Y. H. Yan,¹⁸ H. J. Yang,^{35,h} H. X. Yang,¹ L. Yang,⁵⁵ Y. H. Yang,³⁰ Y. X. Yang,¹¹ M. Ye,^{1,40} M. H. Ye,⁷ J. H. Yin,¹ Z. Y. You,⁴¹ B. X. Yu,^{1,40,44} C. X. Yu,³¹ J. S. Yu,²⁷ C. Z. Yuan,^{1,44} Y. Yuan,¹ A. Yuncu,^{43b,a} A. A. Zafar,⁵² Y. Zeng,¹⁸ Z. Zeng,^{50,40} B. X. Zhang,¹ B. Y. Zhang,^{1,40} C. C. Zhang,¹ D. H. Zhang,¹ H. H. Zhang,⁴¹ H. Y. Zhang,^{1,40} J. Zhang,^{1,44} J. L. Zhang,¹ J. Q. Zhang,¹ J. W. Zhang,^{1,40,44} J. Y. Zhang,¹ J. Z. Zhang,^{1,44} K. Zhang,^{1,44} L. Zhang,⁴² S. Q. Zhang,³¹ X. Y. Zhang,³⁴ Y. H. Zhang,^{1,40} Y. T. Zhang,^{50,40} Yang Zhang,¹ Yao Zhang,¹ Yu Zhang,⁴⁴ Z. H. Zhang,⁶ Z. P. Zhang,⁵⁰ Z. Y. Zhang,⁵⁵ G. Zhao,¹ J. W. Zhao,^{1,40} J. Y. Zhao,^{1,44} J. Z. Zhao,^{1,40} Lei Zhao,^{50,40} Ling Zhao,¹

M. G. Zhao,³¹ Q. Zhao,¹ S. J. Zhao,⁵⁷ T. C. Zhao,¹ Y. B. Zhao,^{1,40} Z. G. Zhao,^{50,40} A. Zhemchugov,^{24,b} B. Zheng,⁵¹
 J. P. Zheng,^{1,40} Y. H. Zheng,⁴⁴ B. Zhong,²⁹ L. Zhou,^{1,40} X. Zhou,⁵⁵ X. K. Zhou,^{50,40} X. R. Zhou,^{50,40} X. Y. Zhou,¹
 Y. X. Zhou,¹² J. Zhu,³¹ J. Zhu,⁴¹ K. Zhu,¹ K. J. Zhu,^{1,40,44} S. Zhu,¹ S. H. Zhu,⁴⁹ X. L. Zhu,⁴²
 Y. C. Zhu,^{50,40} Y. S. Zhu,^{1,44} Z. A. Zhu,^{1,44} J. Zhuang,^{1,40} B. S. Zou,¹ and J. H. Zou¹

(BESIII Collaboration)

- ¹*Institute of High Energy Physics, Beijing 100049, People's Republic of China*
²*Beihang University, Beijing 100191, People's Republic of China*
³*Beijing Institute of Petrochemical Technology, Beijing 102617, People's Republic of China*
⁴*Bochum Ruhr-University, D-44780 Bochum, Germany*
⁵*Carnegie Mellon University, Pittsburgh, Pennsylvania 15213, USA*
⁶*Central China Normal University, Wuhan 430079, People's Republic of China*
⁷*China Center of Advanced Science and Technology, Beijing 100190, People's Republic of China*
⁸*COMSATS Institute of Information Technology, Lahore, Defence Road, Off Raiwind Road, 54000 Lahore, Pakistan*
⁹*G.I. Budker Institute of Nuclear Physics SB RAS (BINP), Novosibirsk 630090, Russia*
¹⁰*GSI Helmholtzcentre for Heavy Ion Research GmbH, D-64291 Darmstadt, Germany*
¹¹*Guangxi Normal University, Guilin 541004, People's Republic of China*
¹²*Guangxi University, Nanning 530004, People's Republic of China*
¹³*Hangzhou Normal University, Hangzhou 310036, People's Republic of China*
¹⁴*Helmholtz Institute Mainz, Johann-Joachim-Becher-Weg 45, D-55099 Mainz, Germany*
¹⁵*Henan Normal University, Xinxiang 453007, People's Republic of China*
¹⁶*Henan University of Science and Technology, Luoyang 471003, People's Republic of China*
¹⁷*Huangshan College, Huangshan 245000, People's Republic of China*
¹⁸*Human University, Changsha 410082, People's Republic of China*
¹⁹*Indiana University, Bloomington, Indiana 47405, USA*
^{20a}*INFN Laboratori Nazionali di Frascati, I-00044, Frascati, Italy*
^{20b}*INFN and University of Perugia, I-06100, Perugia, Italy*
^{21a}*INFN Sezione di Ferrara, I-44122, Ferrara, Italy*
^{21b}*University of Ferrara, I-44122, Ferrara, Italy*
²²*Institute of Physics and Technology, Peace Ave. 54B, Ulaanbaatar 13330, Mongolia*
²³*Johannes Gutenberg University of Mainz, Johann-Joachim-Becher-Weg 45, D-55099 Mainz, Germany*
²⁴*Joint Institute for Nuclear Research, 141980 Dubna, Moscow region, Russia*
²⁵*Justus-Liebig-Universität Giessen, II. Physikalisches Institut, Heinrich-Buff-Ring 16, D-35392 Giessen, Germany*
²⁶*KVI-CART, University of Groningen, NL-9747 AA Groningen, Netherlands*
²⁷*Lanzhou University, Lanzhou 730000, People's Republic of China*
²⁸*Liaoning University, Shenyang 110036, People's Republic of China*
²⁹*Nanjing Normal University, Nanjing 210023, People's Republic of China*
³⁰*Nanjing University, Nanjing 210093, People's Republic of China*
³¹*Nankai University, Tianjin 300071, People's Republic of China*
³²*Peking University, Beijing 100871, People's Republic of China*
³³*Seoul National University, Seoul, 151-747 Korea*
³⁴*Shandong University, Jinan 250100, People's Republic of China*
³⁵*Shanghai Jiao Tong University, Shanghai 200240, People's Republic of China*
³⁶*Shanxi University, Taiyuan 030006, People's Republic of China*
³⁷*Sichuan University, Chengdu 610064, People's Republic of China*
³⁸*Soochow University, Suzhou 215006, People's Republic of China*
³⁹*Southeast University, Nanjing 211100, People's Republic of China*
⁴⁰*State Key Laboratory of Particle Detection and Electronics, Beijing 100049, Hefei 230026, People's Republic of China*
⁴¹*Sun Yat-Sen University, Guangzhou 510275, People's Republic of China*
⁴²*Tsinghua University, Beijing 100084, People's Republic of China*
^{43a}*Ankara University, 06100 Tandogan, Ankara, Turkey*
^{43b}*Istanbul Bilgi University, 34060 Eyup, Istanbul, Turkey*
^{43c}*Uludag University, 16059 Bursa, Turkey*
^{43d}*Near East University, Nicosia, North Cyprus, Mersin 10, Turkey*
⁴⁴*University of Chinese Academy of Sciences, Beijing 100049, People's Republic of China*
⁴⁵*University of Hawaii, Honolulu, Hawaii 96822, USA*
⁴⁶*University of Jinan, Jinan 250022, People's Republic of China*
⁴⁷*University of Minnesota, Minneapolis, Minnesota 55455, USA*

⁴⁸University of Muenster, Wilhelm-Klemm-Str. 9, 48149 Muenster, Germany

⁴⁹University of Science and Technology Liaoning, Anshan 114051, People's Republic of China

⁵⁰University of Science and Technology of China, Hefei 230026, People's Republic of China

⁵¹University of South China, Hengyang 421001, People's Republic of China

⁵²University of the Punjab, Lahore-54590, Pakistan

^{53a}University of Turin, I-10125, Turin, Italy

^{53b}University of Eastern Piedmont, I-15121, Alessandria, Italy

^{53c}INFN, I-10125, Turin, Italy

⁵⁴Uppsala University, Box 516, SE-75120 Uppsala, Sweden

⁵⁵Wuhan University, Wuhan 430072, People's Republic of China

⁵⁶Zhejiang University, Hangzhou 310027, People's Republic of China

⁵⁷Zhengzhou University, Zhengzhou 450001, People's Republic of China



(Received 17 February 2018; revised manuscript received 26 September 2018; published 26 October 2018)

Using a data sample corresponding to an integrated luminosity of 2.93 fb^{-1} taken at a center-of-mass energy of 3.773 GeV with the BESIII detector operated at the BEPCII collider, we perform an analysis of the semileptonic decays $D^{0(+)} \rightarrow \pi^{-(0)} \mu^+ \nu_\mu$. The branching fractions of $D^0 \rightarrow \pi^- \mu^+ \nu_\mu$ and $D^+ \rightarrow \pi^0 \mu^+ \nu_\mu$ are measured to be $(0.272 \pm 0.008_{\text{stat}} \pm 0.006_{\text{syst}})\%$ and $(0.350 \pm 0.011_{\text{stat}} \pm 0.010_{\text{syst}})\%$, respectively, where the former is of much improved precision compared to previous results and the latter is determined for the first time. Using these results along with previous BESIII measurements of $D^{0(+)} \rightarrow \pi^{-(0)} e^+ \nu_e$, we calculate the branching fraction ratios to be $\mathcal{R}^0 \equiv \mathcal{B}_{D^0 \rightarrow \pi^- \mu^+ \nu_\mu} / \mathcal{B}_{D^0 \rightarrow \pi^- e^+ \nu_e} = 0.922 \pm 0.030_{\text{stat}} \pm 0.022_{\text{syst}}$ and $\mathcal{R}^+ \equiv \mathcal{B}_{D^+ \rightarrow \pi^0 \mu^+ \nu_\mu} / \mathcal{B}_{D^+ \rightarrow \pi^0 e^+ \nu_e} = 0.964 \pm 0.037_{\text{stat}} \pm 0.026_{\text{syst}}$, which are compatible with the theoretical expectation of lepton flavor universality within 1.7σ and 0.5σ , respectively. We also examine the branching fraction ratios in different four-momentum transfer square regions, and find no significant deviations from the standard model predictions.

DOI: [10.1103/PhysRevLett.121.171803](https://doi.org/10.1103/PhysRevLett.121.171803)

In the standard model (SM), the couplings of leptons to gauge bosons are expected to be independent of lepton flavors. This property is known as lepton flavor universality (LFU) [1–5]. Tests of LFU with semileptonic (SL) decays of pseudoscalar mesons provide powerful probes of new physics beyond the SM. In recent years, BABAR, Belle and LHCb experiments reported tests of LFU in various SL B decays. The measured branching fraction (BF) ratios $\mathcal{B}_{B \rightarrow \bar{D}^{(*)} \tau^+ \nu_\tau} / \mathcal{B}_{B \rightarrow \bar{D}^{(*)} \ell^+ \nu_\ell}$ ($\ell = \mu, e$) [6–11] and $\mathcal{B}_{B \rightarrow K^{(*)} \mu^+ \mu^-} / \mathcal{B}_{B \rightarrow K^{(*)} e^+ e^-}$ [12,13] deviate from the SM predictions by 1.6–2.7 and 2.1–2.6 standard deviations, respectively. In view of this, tests of LFU in the charm sector using the SL D decays are important complementary tests.

This Letter presents tests of LFU in $D^{0(+)} \rightarrow \pi^{-(0)} \ell^+ \nu_\ell$ decays [14] at BESIII. Recently, the Cabibbo-favored decays $D^{0(+)} \rightarrow \bar{K} \ell^+ \nu_\ell$ were precisely studied at BESIII, and the measured BF ratios (BFRs) $\mathcal{B}_{D \rightarrow \bar{K} \mu^+ \nu_\mu} / \mathcal{B}_{D \rightarrow \bar{K} e^+ \nu_e}$ are compatible with the SM expectations [15–18]. Nevertheless, tension between previous measurement and the SM prediction for the Cabibbo-

suppressed decays $D^0 \rightarrow \pi^- \ell^+ \nu_\ell$ is found. In the SM, the BFRs $\mathcal{R}_{\text{LFU}}^{0(+)} = \mathcal{B}_{D^{0(+)} \rightarrow \pi^{-(0)} \mu^+ \nu_\mu} / \mathcal{B}_{D^{0(+)} \rightarrow \pi^{-(0)} e^+ \nu_e}$ are expected to be 0.985 ± 0.002 [19], which deviates from unity due to different phase space available to the two processes. With the world-average values of $\mathcal{B}_{D^0 \rightarrow \pi^- \mu^+ \nu_\mu}$ and $\mathcal{B}_{D^0 \rightarrow \pi^- e^+ \nu_e}$ [20], $\mathcal{R}_{\text{LFU}}^0$ is 17% lower than the SM prediction, corresponding to 2.1 standard deviations. Currently, the most precise measurements of $\mathcal{B}_{D^{0(+)} \rightarrow \pi^{-(0)} e^+ \nu_e}$ have reached an accuracy better than 3% [15,16]. However, the world-average value of $\mathcal{B}_{D^0 \rightarrow \pi^- \mu^+ \nu_\mu}$ has a large relative uncertainty of 10% [20–22], and the decay $D^+ \rightarrow \pi^0 \mu^+ \nu_\mu$ has not been measured. To clarify this tension, it is crucial to precisely measure $\mathcal{B}_{D^{0(+)} \rightarrow \pi^{-(0)} \mu^+ \nu_\mu}$.

The analysis is performed by using a data sample corresponding to an integrated luminosity of 2.93 fb^{-1} [23] taken at a center-of-mass energy of $\sqrt{s} = 3.773 \text{ GeV}$ with the BESIII detector. Details about the design and performance of the BESIII detector are given in Ref. [24]. A GEANT4-based [25] Monte Carlo (MC) simulation software package, which includes a description of the detector geometry and its response, is used to determine the detection efficiency and to estimate potential backgrounds. An “inclusive” MC sample corresponding to about 10 times the luminosity of data is produced at $\sqrt{s} = 3.773 \text{ GeV}$. It includes the $D^0 \bar{D}^0$, $D^+ D^-$, and non- $D \bar{D}$ decays of $\psi(3770)$, the initial state radiation (ISR) production of $\psi(3686)$ and J/ψ , and the $q \bar{q}$ ($q = u, d, s$) continuum

process, along with Bhabha scattering, $\mu^+\mu^-$ and $\tau^+\tau^-$ events. The production of $\psi(3770)$ is simulated by the MC generator KKMC [26]. The measured decay modes of the charmoniums are generated using EVTGEN [27] with the BF's reported in Ref. [28], and the remaining decay modes are generated using LUNDCHARM [29]. The signal $D^{0(+)} \rightarrow \pi^{-(0)}\mu^+\nu_\mu$ decays are simulated incorporating the modified pole model [30], where the parameters of vector and scalar hadronic form factors (HFFs) are taken from Refs. [15,16,31]. The ISR effects [32] and final state radiation (FSR) effects of all particles [33] have been included in the event generation.

At $\sqrt{s} = 3.773$ GeV, the $\psi(3770)$ resonance decays mainly into a $D\bar{D}$ pair. Throughout the text, D refers to $D^0(D^+)$ and \bar{D} refers to $\bar{D}^0(D^-)$ unless stated explicitly. If a \bar{D} meson [called single-tag (ST) \bar{D} meson] is fully reconstructed, the presence of a D meson is guaranteed. Thus, in the system recoiling against a ST \bar{D} meson, the SL decay $D^{0(+)} \rightarrow \pi^{-(0)}\mu^+\nu_\mu$ [called double-tag (DT) event] can be selected. In this analysis, the ST \bar{D}^0 mesons are reconstructed using three hadronic decay modes: $K^+\pi^-$, $K^+\pi^-\pi^0$ and $K^+\pi^-\pi^+\pi^-$, while the ST D^- mesons are reconstructed using six hadronic decay modes: $K^+\pi^-\pi^-$, $K_S^0\pi^-$, $K^+\pi^-\pi^-\pi^0$, $K_S^0\pi^-\pi^0$, $K_S^0\pi^+\pi^-\pi^-$, and $K^+K^-\pi^-$. The BF of $D^{0(+)} \rightarrow \pi^{-(0)}\mu^+\nu_\mu$ is determined according to

$$\mathcal{B}_{D^{0(+)} \rightarrow \pi^{-(0)}\mu^+\nu_\mu} = N_{\text{DT}}^{0(+)} / (N_{\text{ST}}^{0(+)} \epsilon_{\pi\mu\nu}^{0(+)}), \quad (1)$$

where $N_{\text{ST}}^{0(+)}$ and $N_{\text{DT}}^{0(+)}$ are the ST and DT yields in data, $\epsilon_{\pi\mu\nu}^{0(+)}$ is the signal efficiency of finding $D^{0(+)} \rightarrow \pi^{-(0)}\mu^+\nu_\mu$ events in the presence of a ST \bar{D} meson. Here, $\epsilon_{\pi\mu\nu}^{0(+)} = \sum_k (N_{\text{ST}}^k \epsilon_{\text{DT}}^k) / (N_{\text{ST}}^{0(+)} \epsilon_{\text{ST}}^{0(+)})$, where N_{ST}^k and ϵ_{ST}^k are the ST yield and the ST[DT] efficiency of the k th tag mode, respectively.

All charged tracks are required to be within a polar-angle range of $|\cos\theta| < 0.93$. Except for those from K_S^0 decays, the good charged tracks are required to come from the interaction region defined by $V_{xy} < 1$ cm and $|V_z| < 10$ cm, where V_{xy} and $|V_z|$ are the distances of closest approach of the reconstructed track to the interaction point (IP) in the xy plane and the z direction (along the beam), respectively. Charged particle identification (PID) is performed by combining the time-of-flight information with the specific ionization energy loss measured in the main drift chamber. The information of the electromagnetic calorimeter (EMC) is also included to identify muon candidates. Combined confidence levels (CL_e , CL_μ , CL_π , and CL_K) are calculated individually. The kaon and pion are required to satisfy $CL_K > CL_\pi$ and $CL_\pi > CL_K$, respectively, while muon candidates are selected with $CL_\mu > 0.001$, $CL_\mu > CL_e$, and $CL_\mu > CL_K$. Additionally, muon candidates are required to deposit an energy in the EMC within the range (0.1,0.3) GeV and to satisfy a polar angle and momentum dependent hit depth

criterion in the muon counter (MUC) [34]; these criteria suppress the number of pions misidentified as muons. The K_S^0 candidate is reconstructed from two oppositely charged tracks with $|V_z| < 20$ cm. These two charged tracks are assumed to be pions (without PID), constrained to a common vertex and are required to have an invariant mass satisfying $|M_{\pi^+\pi^-} - M_{K_S^0}| < 12$ MeV/ c^2 , where $M_{K_S^0}$ is the K_S^0 nominal mass [20]. A selected K_S^0 candidate must have a decay length larger than 2 times of the vertex resolution away from the IP. Photon candidates are selected from the shower clusters in the EMC that are not associated with a charged track. The shower time is required to be within 700 ns of the event start time, its energy is required to be greater than 25 (50) MeV in the EMC barrel (end cap) region [24]. The opening angle between the shower and any charged tracks must be greater than 10° . A π^0 candidate is reconstructed from a $\gamma\gamma$ pair with an invariant mass $M_{\gamma\gamma}$ within (0.115,0.150) GeV/ c^2 . A kinematic fit constraining $M_{\gamma\gamma}$ to the π^0 nominal mass [20] is imposed to improve its momentum resolution.

The ST \bar{D} mesons are identified by the energy difference $\Delta E \equiv E_{\bar{D}} - E_{\text{beam}}$ and the beam-constrained mass $M_{\text{BC}} \equiv \sqrt{E_{\text{beam}}^2/c^4 - |\vec{p}_{\bar{D}}|^2/c^2}$. Here, E_{beam} is the beam energy, $\vec{p}_{\bar{D}}$ and $E_{\bar{D}}$ are the momentum and energy of the \bar{D} candidate in the e^+e^- rest frame. For each ST mode, if there are multiple candidates in an event, only the one with the smallest $|\Delta E|$ is kept. The ST candidates are required to have $\Delta E \in (-55, 40)$ MeV and $(-25, 25)$ MeV for the modes with and without a π^0 in the final states, respectively. For the ST candidates of $\bar{D}^0 \rightarrow K^+\pi^-$, the backgrounds from cosmic rays and Bhabha events are further rejected using the requirements described in Ref. [35]. After the above selection criteria, the ST yields are obtained by performing maximum likelihood fits to the M_{BC} distributions for

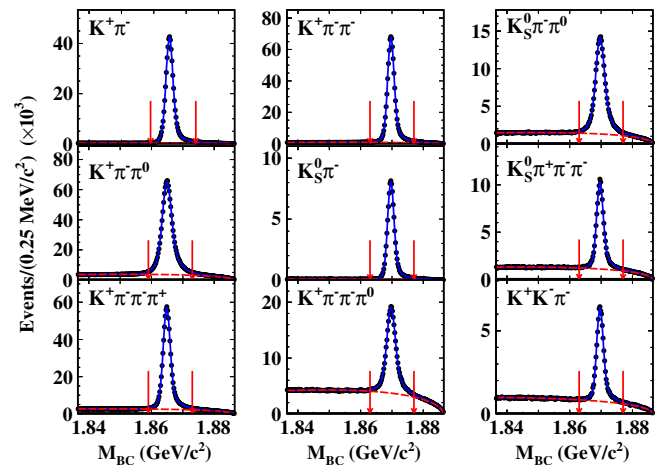


FIG. 1. Fits to the M_{BC} distributions of the ST \bar{D}^0 (left column) and D^- (middle and right columns) modes. The dots with error bars are data. The blue solid and red dashed curves are the fit results and the fitted backgrounds. The signal region is between the red arrows.

individual ST modes, as shown in Fig. 1. In the fits, the \bar{D} signal is modeled by a MC-simulated shape convolved with a double Gaussian function that describes any resolution difference between data and MC simulation. For individual tags, the peaks and resolutions of the convolved Gaussian functions fall in the regions of $(-0.3, 0.3)$ MeV/c^2 and $(0.7, 3.2)$ MeV/c^2 , respectively. The combinatorial background is described by an ARGUS function [36]. The candidates in the M_{BC} signal regions, defined as $(1.859, 1.873)$ GeV/c^2 and $(1.863, 1.877)$ GeV/c^2 for \bar{D}^0 and D^- , respectively, are kept for further analysis.

In the part of the event recoiling against the ST \bar{D} meson, the SL decay candidate is selected from the remaining tracks that have not been used for tag reconstruction. Events containing a muon candidate, with opposite charge to the ST \bar{D} candidate, and a $\pi^{-(0)}$ candidate are considered as SL $D^{0(+)}$ decays. We require there are no additional charged tracks in the event. The potential backgrounds from $D^0 \rightarrow K^- \pi^+$, $D^{0(+)} \rightarrow \pi^{-(0)} \pi^+$ and $D^{0(+)} \rightarrow \pi^{-(0)} \pi^+ \pi^0 / \eta / \bar{K}^0$ are suppressed by the optimized requirements of $M_{\pi^{-(0)}\mu^+} < 1.7$ GeV/c^2 and $E_{\text{max}}^{\text{extra}\gamma} < 0.07$ GeV , where $M_{\pi^{-(0)}\mu^+}$ is the $\pi^{-(0)}\mu^+$ invariant mass and $E_{\text{max}}^{\text{extra}\gamma}$ is the maximum energy of any additional photon candidates unused in the DT reconstruction. The relative efficiencies of the requirements on $M_{\pi^{-(0)}\mu^+}$ and $E_{\text{max}}^{\text{extra}\gamma}$ are approximately 99% and 70%, respectively. To further reject the peaking backgrounds of $D^0 \rightarrow K_S^0(\pi^+\pi^-)\pi^0$ and $D^+ \rightarrow \bar{K}^0\pi^+$ for $D^0 \rightarrow \pi^-\mu^+\nu_\mu$ and $D^+ \rightarrow \pi^0\mu^+\nu_\mu$, we require $M_{\pi^-\mu^+}$ and $M_{D^-\mu^+}^{\text{rec}}$ ($D^-\mu^+$ recoil mass) to be outside the ranges $(0.46, 0.50)$ GeV/c^2 and $(0.45, 0.55)$ GeV/c^2 , respectively. The undetected neutrino is inferred from the variable $M_{\text{miss}}^2 \equiv E_{\text{miss}}^2/c^4 - |\vec{p}_{\text{miss}}|^2/c^2$, which peaks at zero for signal events. Here E_{miss} and $|\vec{p}_{\text{miss}}|$ are the missing energy and momentum calculated by $E_{\text{miss}} \equiv E_{\text{beam}} - E_{\pi^{-(0)}} - E_{\mu^+}$ and $\vec{p}_{\text{miss}} \equiv \vec{p}_D - \vec{p}_{\pi^{-(0)}} - \vec{p}_{\mu^+}$, in which $E_{\pi^{-(0)}}(E_{\mu^+})$ and $\vec{p}_{\pi^{-(0)}}(\vec{p}_{\mu^+})$ are the energy and momentum of $\pi^{-(0)}$ (μ^+) in the rest frame of e^+e^- system. Furthermore, $\vec{p}_D \equiv (-\hat{p}_D)\sqrt{E_{\text{beam}}^2/c^2 - M_D^2}$ is the momentum of D meson, where \hat{p}_D is the momentum direction of the ST \bar{D} meson and M_D is the D nominal mass [20].

Figure 2 shows the M_{miss}^2 distributions of the selected DT candidates for $D^0 \rightarrow \pi^-\mu^+\nu_\mu$ and $D^+ \rightarrow \pi^0\mu^+\nu_\mu$. Both the candidate events contain two peaks corresponding to the $D^{0(+)} \rightarrow \pi^{-(0)}\mu^+\nu_\mu$ signals and the $D^{0(+)} \rightarrow \pi^{-(0)}\pi^+\bar{K}^0$ backgrounds (named BKGI) at zero and 0.25 GeV^2/c^4 , respectively. MC studies indicate that the small peaking backgrounds from decays $D^0 \rightarrow K^- \pi^+$, $D^{0(+)} \rightarrow \pi^{-(0)}\pi^+$, and $D^{0(+)} \rightarrow \pi^{-(0)}\pi^+\pi^0$ (named BKGII) peak around 0.02 GeV^2/c^4 , under the right side of the signal. The DT signal yields are determined by performing unbinned maximum likelihood fits on the M_{miss}^2 distributions. In the fits, the signals, the peaking backgrounds of BKGI and

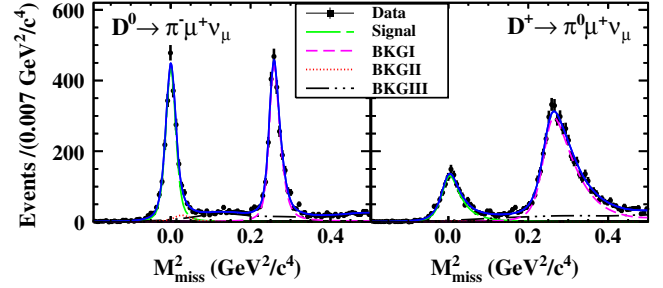


FIG. 2. Fits to the M_{miss}^2 distributions of the DT candidates. The dots with error bars are data. The blue solid, green long dashed, pink dashed, red dotted and black dot-dashed curves represent the overall fit results, the SL signals, the BKGI, BKGII and BKGIII components (see text), respectively.

BKGII and other nonpeaking backgrounds (named BKGIII) are described by the corresponding MC-simulated shapes. The signal, BKGI, and BKGII shapes are smeared with Gaussian functions with free parameters to take into account the resolution difference between data and MC simulation. The parameters of the Gaussian function for BKGII are the same as those for the signal, while those for BKGI can be different. All but one of the BKGII peaking background yields are fixed to the values from MC simulation; the exception is the $D^0 \rightarrow \pi^+\pi^-\pi^0$ background to the $D^0 \rightarrow \pi^-\mu^+\nu_\mu$ signal, which is determined from data due to its good separation from the signal. All the other background component yields are floated in the fit.

The ST and DT yields, the detection efficiencies and the obtained BF's are shown in Table I. In BF measurements using the DT method, the uncertainties from the ST selection mostly cancel. The relative systematic uncertainties from the different sources considered are shown in Table II. The uncertainty from the ST yield is taken as 0.5% by examining its relative change between data and MC simulation by varying the fit range, signal shape, and end point of the ARGUS function. The efficiencies of μ^+ and π^- tracking (PID) and π^0 reconstruction are verified using $e^+e^- \rightarrow \gamma\mu^+\mu^-$ events and DT $D\bar{D}$ hadronic events, respectively. We assign the uncertainties of π^- tracking (PID), μ^+ tracking (PID), and π^0 reconstruction to be 0.5% (0.5%), 0.5% (0.5%), and 1.0%, respectively. The uncertainty related to the choice of the $E_{\text{max}}^{\text{extra}\gamma}$ requirement is assigned by analyzing the control sample

TABLE I. ST and DT yields, signal efficiencies in the M_{BC} signal regions, and the obtained BF's. The numbers in the first and second brackets are the statistical and systematic uncertainties in the last two digits, respectively. The efficiencies do not include $\mathcal{B}_{\pi^0 \rightarrow \gamma\gamma}$. See Supplemental Material [37] for tag dependent numbers.

Mode	$N_{\text{ST}}^{0(+)} (\times 10^4)$	$N_{\text{DT}}^{0(+)}$	$\epsilon_{\pi\mu\nu}^{0(+)} (\%)$	$\mathcal{B}_{D \rightarrow \pi\mu\nu} (\%)$
$\pi^-\mu^+\nu_\mu$	232.1(02)	2265(63)	35.82(08)	0.272(08)(06)
$\pi^0\mu^+\nu_\mu$	152.2(02)	1335(42)	25.36(07)	0.350(11)(10)

TABLE II. Relative systematic uncertainties in BF measurements.

Source (%)	$\mathcal{B}_{\pi\mu\nu}^0$	$\mathcal{B}_{\pi\mu\nu}^+$
ST yields	0.5	0.5
μ^+ tracking	0.5	0.5
μ^+ PID	0.5	0.5
π^- tracking	0.5	...
π^- PID	0.5	...
π^0 reconstruction	...	1.0
$E_{\max}^{\text{extra}\gamma}$ requirement	1.2	1.7
$M_{\pi\mu^+}$ requirement	0.4	0.9
K_S^0 veto	...	0.2
M_{miss}^2 fit	1.6	1.4
MC statistics	0.3	0.3
MC generator	0.3	0.3
FSR effect	0.3	0.3
Total	2.4	2.8

$D^{0(+)} \rightarrow \pi^{-(0)} e^+ \nu_e$; it is 1.2% (1.7%) for the $D^{0(+)}$ decay. The uncertainty associated with the $M_{\pi\mu^+}$ requirement is investigated by using the alternative requirements of 1.65 GeV/ c^2 or 1.75 GeV/ c^2 . The uncertainty due to the K_S^0 veto is estimated by varying the $M_{\pi^-\mu^+}$ ($M_{D^-\mu^+}^{\text{rec}}$) requirement by ± 0.01 GeV/ c^2 . The changes to the measured BFs with the different requirements are taken as the systematic uncertainties. The uncertainties related to the M_{miss}^2 fits are investigated by varying the fit ranges by $\pm 0.025(0.050)$ GeV $^2/c^4$ for $D^{0(+)}$ decays, and with different parametrizations of signals, combinatorial and peaking backgrounds. The effects due to signal shapes are estimated with different requirements on the MC-truth matched signal shapes. The relative magnitudes of the dominant combinatorial background components in BKGIII are varied by $\pm 20\%$. The fixed magnitudes of the dominant peaking backgrounds in BKGII are changed according to the BF uncertainties [20], the limited MC statistics of background channels, and the data-MC differences of the rates of misidentifying K^- as π^- and π^+ as μ^+ . The maximum changes of BFs are taken as their respective uncertainties. The uncertainties due to limited MC statistics are 0.3% for both decays. The uncertainty related to MC generator assumptions is estimated to be 0.3% via comparing the DT efficiencies by varying the quoted vector HFF parameters by ± 1 standard deviation and replacing the nominal scalar HFF model with the simple pole model [30]. The uncertainty due to FSR effect is assigned as 0.3%, which is obtained by comparing the nominal DT efficiency to that when the FSR photon probability is changed by $\pm 20\%$. The total systematic uncertainty is the quadratic sum of the individual contributions.

Combining the $\mathcal{B}_{D^{0(+)} \rightarrow \pi^{-(0)} \mu^+ \nu_\mu}$ measured in this work with previous BESIII measurements [15,16] $\mathcal{B}_{D^0 \rightarrow \pi^- e^+ \nu_e} = (0.295 \pm 0.004_{\text{stat}} \pm 0.003_{\text{syst}})\%$ and $\mathcal{B}_{D^+ \rightarrow \pi^0 e^+ \nu_e} = (0.363 \pm 0.008_{\text{stat}} \pm 0.005_{\text{syst}})\%$, we obtain $\mathcal{R}_{\text{LFU}}^0 = 0.922 \pm 0.030_{\text{stat}} \pm 0.022_{\text{syst}}$ and $\mathcal{R}_{\text{LFU}}^+ = 0.964 \pm 0.037_{\text{stat}} \pm 0.026_{\text{syst}}$. Here, the systematic uncertainties in ST yields,

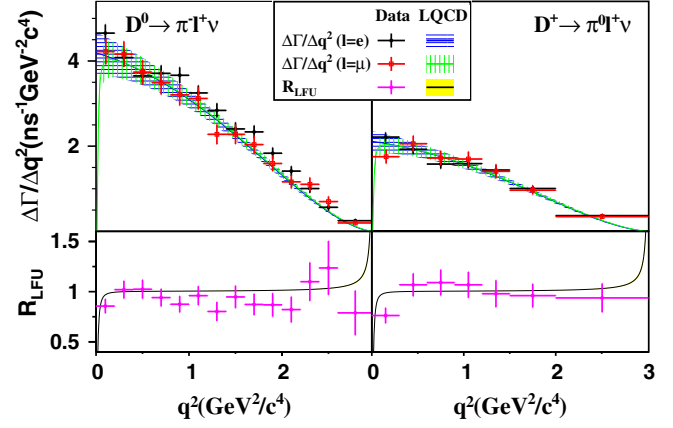


FIG. 3. $\Delta\Gamma_i^{0(+)} / \Delta q^2$ of $D^{0(+)} \rightarrow \pi^{-(0)} e^+ \nu_e$ (top) and $\mathcal{R}_{\text{LFU}}^{0(+)}$ (bottom) in various q^2 bins. The calculations of $\Delta\Gamma_i^{0(+)} / \Delta q^2$ of $D^{0(+)} \rightarrow \pi^{-(0)} e^+ \nu_e$ are quoted from Refs. [15,16]. Data are shown as dots with error bars, where the uncertainties are combined from statistical and systematic errors, and the uncertainties in $\mathcal{R}_{\text{LFU}}^0$ are dominated by the statistical uncertainties of semi-muonic modes. The blue, green and black curves with bands show the LQCD predictions with uncertainties, using the equations and HFF parameters described in Refs. [19,38], where the theoretical uncertainties in $\mathcal{R}_{\text{LFU}}^{0(+)}$ are tiny due to strong correlation of the form factors.

π^- tracking and PID, and π^0 reconstruction cancel, and an additional uncertainty of 0.5% is included to take into account different FSR effects for electron and muon. The measured values of $\mathcal{R}_{\text{LFU}}^{0(+)}$ coincide with the SM expectation 0.985 ± 0.002 [19] within $1.7\sigma(0.5\sigma)$.

The BFRs $\mathcal{R}_{\text{LFU}}^{0(+)}$ are obtained in the full q^2 (four-momentum transfer square of $\mu^+ \nu_\mu$) region. To investigate the q^2 dependence of $\mathcal{R}_{\text{LFU}}^{0(+)}$, we examine BFRs in different q^2 ranges. Using the method described in Refs. [15,16], the partial width of $D^{0(+)} \rightarrow \pi^{-(0)} \mu^+ \nu_\mu$ in the i th q^2 bin is calculated by

$$\Delta\Gamma_i^{0(+)} = N_i^{0(+)} / (\tau_{D^{0(+)}} N_{\text{ST}}^{0(+)}), \quad (2)$$

where $\tau_{D^{0(+)}}$ is the lifetime of the $D^{0(+)}$ meson, and $N_i^{0(+)}$ is the produced DT yield in the i th q^2 bin, calculated by $N_i^{0(+)} = \sum_j (\epsilon_{0(+)}^{-1})_{ij} M_j^{0(+)}$. Here $M_j^{0(+)}$ is the observed DT yield in the j th q^2 bin, $\epsilon_{0(+)}^{-1}$ is the efficiency matrix and $(\epsilon_{0(+)}^{-1})_{ij}$ are the elements of a matrix that describes the efficiency and smearing across q^2 bins. See Supplemental Material [37] for the observed and produced DT yields, efficiency matrices as well as the partial widths for $D^{0(+)} \rightarrow \pi^{-(0)} \mu^+ \nu_\mu$. Combining with the measured partial widths for $D^{0(+)} \rightarrow \pi^{-(0)} e^+ \nu_e$ in the same q^2 bins [15,16], we obtain $\mathcal{R}_{\text{LFU}}^{0(+)}$ in various q^2 bins. Figure 3 shows $\Delta\Gamma_i^{0(+)} / \Delta q^2$ and $\mathcal{R}_{\text{LFU}}^{0(+)}$ in various q^2 bins, as well as the LQCD predictions for comparison. The measured values

are consistent with the SM predictions within 2σ in most of the q^2 regions.

In summary, using 2.93 fb^{-1} e^+e^- collision data collected at $\sqrt{s} = 3.773\text{ GeV}$ with the BESIII detector, we have measured the BF of $D^0 \rightarrow \pi^-\mu^+\nu_\mu$ and $D^+ \rightarrow \pi^0\mu^+\nu_\mu$. The value of $\mathcal{B}_{D^0 \rightarrow \pi^-\mu^+\nu_\mu}$ is consistent with the world-average value [20] and has much improved precision; $\mathcal{B}_{D^+ \rightarrow \pi^0\mu^+\nu_\mu}$ is determined for the first time. Combining the previous BESIII measurements of $D^{0(+)} \rightarrow \pi^{-(0)}e^+\nu_e$, we calculate the q^2 -integrated and q^2 -dependent BFRs, and find no significant evidence of LFU violation.

The BESIII collaboration thanks the staff of BEPCII and the IHEP computing center for their strong support. Authors thanks S. Simula, L. Riggio, G. Salerno, and Wei Wang for helpful discussions. This work is supported in part by National Key Basic Research Program of China under Contract No. 2015CB856700; National Natural Science Foundation of China (NSFC) under Contracts No. 11235011, No. 11305180, No. 11335008, No. 11375170, No. 11425524, No. 11475123, No. 11475164, No. 11475169, No. 11605196, No. 11605198, No. 11625523, No. 11635010, No. 11705192; the Chinese Academy of Sciences (CAS) Large-Scale Scientific Facility Program; the CAS Center for Excellence in Particle Physics (CCEPP); Joint Large-Scale Scientific Facility Funds of the NSFC and CAS under Contracts No. U1332201, No. U1532101, No. U1532102, No. U1532257, No. U1532258, No. U1732263; CAS under Contracts No. KJCX2-YW-N29, No. KJCX2-YW-N45, and No. QYZDJ-SSW-SLH003; 100 Talents Program of CAS; National 1000 Talents Program of China; INPAC and Shanghai Key Laboratory for Particle Physics and Cosmology; German Research Foundation DFG under Contracts No. Collaborative Research Center CRC 1044, No. FOR 2359; Istituto Nazionale di Fisica Nucleare, Italy; Koninklijke Nederlandse Akademie van Wetenschappen (KNAW) under Contract No. 530-4CDP03; Ministry of Development of Turkey under Contract No. DPT2006K-120470; National Science and Technology fund; The Swedish Research Council; U.S. Department of Energy under Contracts No. DE-FG02-05ER41374, No. DE-SC-0010118, No. DE-SC-0010504, No. DE-SC-0012069; University of Groningen (RuG) and the Helmholtzzentrum fuer Schwerionenforschung GmbH (GSI), Darmstadt; WCU Program of National Research Foundation of Korea under Contract No. R32-2008-000-10155-0.

^aAlso at Bogazici University, 34342 Istanbul, Turkey.

^bAlso at the Moscow Institute of Physics and Technology, Moscow 141700, Russia.

^cAlso at the Functional Electronics Laboratory, Tomsk State University, Tomsk, 634050, Russia.

^dAlso at the Novosibirsk State University, Novosibirsk, 630090, Russia.

^eAlso at the NRC “Kurchatov Institute”, PNPI, 188300, Gatchina, Russia.

^fAlso at Istanbul Arel University, 34295 Istanbul, Turkey.

^gAlso at Goethe University Frankfurt, 60323 Frankfurt am Main, Germany.

^hAlso at Key Laboratory for Particle Physics, Astrophysics and Cosmology, Ministry of Education; Shanghai Key Laboratory for Particle Physics and Cosmology; Institute of Nuclear and Particle Physics, Shanghai 200240, People’s Republic of China.

ⁱGovernment College Women University, Sialkot—51310, Punjab, Pakistan.

^jPresent address: Center for Underground Physics, Institute for Basic Science, Daejeon 34126, Korea.

- [1] X. D. Guo, X. Q. Hao, H. W. Ke, M. G. Zhao, and X. Q. Li, *Chin. Phys. C* **41**, 093107 (2017).
- [2] S. Fajfer, I. Nisandzic, and U. Rojec, *Phys. Rev. D* **91**, 094009 (2015).
- [3] S. Fajfer, J. F. Kamenik, and I. Nisandzic, *Phys. Rev. D* **85**, 094025 (2012).
- [4] S. Fajfer, J. F. Kamenik, I. Nisandzic, and J. Zupan, *Phys. Rev. Lett.* **109**, 161801 (2012).
- [5] M. Bauer and M. Neubert, *Phys. Rev. Lett.* **116**, 141802 (2016).
- [6] J. P. Lees *et al.* (BABAR Collaboration), *Phys. Rev. Lett.* **109**, 101802 (2012).
- [7] J. P. Lees *et al.* (BABAR Collaboration), *Phys. Rev. D* **88**, 072012 (2013).
- [8] A. Matyja *et al.* (Belle Collaboration), *Phys. Rev. Lett.* **99**, 191807 (2007).
- [9] A. Bozek *et al.* (Belle Collaboration), *Phys. Rev. D* **82**, 072005 (2010).
- [10] Y. Sato *et al.* (Belle Collaboration), *Phys. Rev. D* **94**, 072007 (2016).
- [11] R. Aaij *et al.* (LHCb Collaboration), *Phys. Rev. Lett.* **115**, 111803 (2015).
- [12] R. Aaij *et al.* (LHCb Collaboration), *Phys. Rev. Lett.* **113**, 151601 (2014).
- [13] R. Aaij *et al.* (LHCb Collaboration), *J. High Energy Phys.* **08** (2017) 055.
- [14] Throughout the Letter, the charge conjugate processes are implied unless explicitly stated otherwise.
- [15] M. Ablikim *et al.* (BESIII Collaboration), *Phys. Rev. D* **92**, 072012 (2015).
- [16] M. Ablikim *et al.* (BESIII Collaboration), *Phys. Rev. D* **96**, 012002 (2017).
- [17] M. Ablikim *et al.* (BESIII Collaboration), *Eur. Phys. J. C* **76**, 369 (2016).
- [18] M. Ablikim *et al.* (BESIII Collaboration), arXiv:1810.03127.
- [19] L. Riggio, G. Salerno, and S. Simula, *Eur. Phys. J. C* **78**, 501 (2018).
- [20] M. Tanabashi *et al.* (Particle Data Group), *Phys. Rev. D* **98**, 030001 (2018).
- [21] L. Widhalm *et al.* (Belle Collaboration), *Phys. Rev. Lett.* **97**, 061804 (2006).

- [22] J. M. Link *et al.* (FOCUS Collaboration), *Phys. Lett. B* **607**, 51 (2005).
- [23] M. Ablikim *et al.* (BESIII Collaboration), *Chin. Phys. C* **37**, 123001 (2013); *Phys. Lett. B* **753**, 629 (2016).
- [24] M. Ablikim *et al.* (BESIII Collaboration), *Nucl. Instrum. Methods Phys. Res., Sect. A* **614**, 345 (2010).
- [25] S. Agostinelli *et al.* (GEANT4 Collaboration), *Nucl. Instrum. Methods Phys. Res., Sect. A* **506**, 250 (2003).
- [26] S. Jadach, B. F. L. Ward, and Z. Was, *Comput. Phys. Commun.* **130**, 260 (2000); *Phys. Rev. D* **63**, 113009 (2001).
- [27] D. J. Lange, *Nucl. Instrum. Methods A* **462**, 152 (2001); R. G. Ping, *Chin. Phys. C* **32**, 599 (2008).
- [28] K. Nakamura *et al.* (Particle Data Group), *J. Phys. G* **37**, 075021 (2010), and 2011 partial update for the 2012 edition.
- [29] J. C. Chen, G. S. Huang, X. R. Qi, D. H. Zhang, and Y. S. Zhu, *Phys. Rev. D* **62**, 034003 (2000).
- [30] D. Becirevic and A. B. Kaidalov, *Phys. Lett. B* **478**, 417 (2000).
- [31] H. Y. Cheng, C. K. Chua, and C. W. Hwang, *Phys. Rev. D* **69**, 074025 (2004).
- [32] E. A. Kuraev and V. S. Fadin, *Yad. Fiz.* **41**, 733 (1985); [*Sov. J. Nucl. Phys.* **41**, 466 (1985)].
- [33] E. Barberio and Z. Was, *Comput. Phys. Commun.* **79**, 291 (1994).
- [34] Given six momenta a, b, c, d, e , and f , the five momenta ranges are defined as (a, b) , (b, c) , (c, d) , (d, e) , and (e, f) , respectively. Two dimensional ($|\cos \theta_\mu|$ and momentum p_μ) requirement on the hit depth (\mathcal{D}) in the MUC is imposed if $p_\mu > 0.5 \text{ GeV}/c$ [24]. The $|\cos \theta_{\mu,i}|$ is equally divided as $[0.2 \times (i-1), 0.2 \times i]$ ($i = 1, 2, 3, 4$, or 5). In the first three $|\cos \theta_{\mu,i}|$ bins, we require \mathcal{D} greater than 3, $100 \times p_\mu - (55 + 3 \times i)$, 17, $100 \times p_\mu - (68 + 3 \times i)$ and 33 cm for p_μ in the ranges bounded by every neighbour two momenta of $0.50 - 0.58 + 0.03 \times i$, $0.72 + 0.03 \times i$, $0.85 + 0.03 \times i$, $1.01 + 0.03 \times i$ and 1.2 [34], respectively. For the other two $|\cos \theta_{\mu,i}|$ bins, we require \mathcal{D} greater than 9 cm uniformly.
- [35] M. Ablikim *et al.* (BESIII Collaboration), *Phys. Lett. B* **734**, 227 (2014).
- [36] H. Albrecht *et al.* (ARGUS Collaboration), *Phys. Lett. B* **241**, 278 (1990).
- [37] See Supplemental Material at <http://link.aps.org/supplemental/10.1103/PhysRevLett.121.171803> for the tag dependent ST yields and efficiencies, DT efficiencies, and signal efficiencies; the observed DT yields and the produced DT yields; the partial widths for $D^{0(+)} \rightarrow \pi^{-(0)} \mu^+ \nu_\mu$ in various q^2 bins and the efficiency matrices.
- [38] V. Lubicz, L. Riggio, G. Salerno, S. Simula, and C. Tarantino, *Phys. Rev. D* **96**, 054514 (2017).